

**High resolution spectroscopic diagnostic for divertor and
scrape-off layer neutral and impurity emission measurements in
the National Spherical Torus Experiment.**

V. A. Soukhanovskii, A. L. Roquemore, C. H. Skinner,

J. Menard, H. W. Kugel, D. Johnson

Princeton Plasma Physics Laboratory, Princeton, New Jersey

R. Maingi

Oak Ridge National Laboratory, Oak Ridge, Tennessee

S. Sabbagh, F. Paoletti

Columbia University, New York, New York

Abstract

The National Spherical Torus Experiment (NSTX) boundary physics program presently focuses on edge power and particle flow optimization and control in $\beta \geq 25\%$ long pulse L- and H-mode plasmas with high harmonic fast wave heating power up to 6 MW and neutral beam injection power up to 5 MW, with the emphasis on the edge physics implications resulting from the low aspect ratio geometry. To address the particle flux measurements in the divertor and plasma scrape-off layer (SOL) two spectrally filtered one dimensional charged couple device cameras have been fielded. The cameras utilize 2048 pixel 12-bit Dalsa CL-C6 arrays, $f = 85$ mm lenses, and $\Delta\lambda = 1.5$ nm bandpass interference filters. Both cameras provide mm spatial resolution, sub-ms temporal resolution and are spatially and photometrically calibrated. Midplane SOL and divertor brightness profiles of C III and deuterium species

have been obtained in L- and H-mode phases of center stack limited and diverted plasmas. The equilibria reconstructed by EFIT code are found in good agreement with the optical measurements. In-out asymmetries in divertor recycling and carbon fluxes have been observed in L- and H-mode plasmas. No strong systematic dependence of inboard brightness profiles and divertor particle flux in-out asymmetries on magnetic boundary configuration has been found. The analysis of neutral recycling and impurity fluxes using the two dimensional multi-fluid code UEDGE is in progress.

I. INTRODUCTION

Charge-coupled device based visible detectors, hereforth referred to as CCD cameras, have become common imaging diagnostics in high-temperature magnetically confined toroidal plasma experiments in recent years [1], [2], [3]. The assumption of toroidal symmetry enables one to use linear CCD arrays for brightness profile measurements of the edge and divertor regions. Self-scanning one dimensional (1D) CCD arrays provide clear advantages over commonly used photodiode arrays (for example, [4]) in that the achievable spatial resolution is much higher without loss in temporal resolution. This paper describes the use of 1D CCD arrays for divertor and plasma scrape-off layer (SOL) deuterium and carbon brightness profile measurements in the National Spherical Torus Experiment (NSTX). NSTX is a proof of principle spherical torus experiment. It has successfully achieved $\beta_t \geq 30\%$ mega-amp plasmas and routine H-mode operation with confinement times of $\tau_E \simeq 1.5 \times \tau_{ITER98pby2}$ [5]. The boundary physics program presently focuses on edge power and particle flow optimization and control in the L- and H-mode plasmas with high harmonic fast wave heating (HHFW) power up to 6 MW and neutral beam injection (NBI) power up to 5 MW. The specific physics points being addressed are the characterization of the L-H transition, H-mode access conditions, edge localized modes (ELMs), edge parallel and perpendicular particle and heat transport, and advanced wall conditioning techniques, with the emphasis on the

physics implications of the low aspect ratio geometry. Because of the sharp gradients in impurity and neutral emission in the edge and divertor a high resolution imaging diagnostic is especially important: the interpretation of the profiles involves two dimensional fluid modeling which requires the details of impurity and neutral recycling distribution. Two cameras have been fielded at NSTX: one camera, referred to as the MID camera, is mounted at a midplane location with either a tangential or a vertical view of the center stack; the second camera (LDIV camera) is mounted on top of the vacuum vessel with a radial view across the lower divertor. The cameras together with core profile diagnostics, divertor infra-red cameras and divertor tile Langmuir probes provide the basic data necessary for studying edge recycling, core fueling and edge particle flows.

II. CCD ARRAYS

The 1D CCD cameras used on NSTX are the Dalsa CL-C6-2048T self-scanning 2048 pixel arrays. The maximum frame rate is $f = 2.4$ kHz. The data format conforms to the 12-bit RS422 standard. Data requisition of the cameras is controlled by a personal computer (PC) located in NSTX test cell. Image capture is performed by two National Instruments IMAQ PCI-1424 framegrabbers triggered by a TTL pulse. LabView data acquisition software is used for camera control, PC data management and integration into the master clock cycle and MDS Plus data system. Both cameras and the PC are located in NSTX test cell, and are immune to radio frequency waves and energetic particles related to HHFW and NBI operation. The photometric responsivity of the array is 618 DN/(nJ/cm), and the dynamic range is 1420:1. Both cameras are equipped with the Nikon F-mount 85 mm diameter $f/1.8$ lenses. Narrow bandpass $\Delta\lambda \simeq 1.5$ nm interference filters and neutral density filters are mounted directly on the lens front. The interference filter transmission is $T \leq 0.5$. Because of the limited acceptance angle of the interference filter, the effective f -number of the lens and filter is $f/5.6$. The filters are used for selective measurements of deuterium (D_α $\lambda = 6561$ Å), C III ($\lambda = 4650$ Å), and He II ($\lambda = 4686$ Å) brightness profiles. A visible spectrometer

is used to verify that the measured profiles are not contaminated by atomic or molecular spectral lines within the filter bandpass.

The spatial calibration is performed *in situ* during vacuum vessel maintenance using small lights mounted directly on the divertor or center stack tiles whose positions can be measured with high accuracy. However, the cameras are removed from the vessel after the calibration because the in-vessel plasma facing components are baked to 300 degrees C in preparation for plasma operations. A developed interim procedure allows us to maintain the camera position so that the uncertainty in the individual pixel line of sight is presently limited to 5 mm. The procedure is being improved to further reduce the calibration uncertainty. Laboratory tests reproducing the cameras mounting geometry demonstrated that the achievable spatial resolution is better than 1 mm. The photometric calibration of the camera and filters is accomplished in the laboratory using a Labspere absolutely calibrated light source. This is adequate for the MID camera, however the LDIV camera view may be vignetted by the edges of the rectangular viewing slot cut in the divertor and passive plates. The linear spatial responsivity of the cameras was verified *in situ* by moving a D_α lamp across their field of view, however the extent of the vignetting of the LDIV camera view will be further investigated.

The interpretation of the measured brightnesses $B = (4\pi)^{-1} \int_L \varepsilon dl$ where the integration of the local emissivity ε is performed along the line of sight L , requires the knowledge of local electron temperature and density distributions. As the data become available, the analysis will proceed as follows. Divertor D_α brightness profiles obtained with the LDIV camera will be simulated and used as a constraint for edge transport modeling with UEDGE code [6]. The inboard emissivity profiles ε are obtained using an algebraic inversion algorithm assuming toroidal symmetry of the equal emissivity shells: $\varepsilon_j = \sum_i L_{ij}^{-1} B_i$, where ε_j is the j -th shell emissivity, L_{ij} is the length of the i th chord in the j th shell, and the measured i th chord brightness is $B_i = \sum_j \varepsilon_j L_{ij}$. Neutral and impurity densities are derived from the emissivities using a collisional-radiative model.

III. RESULTS

A. Plasma boundary configurations

Inner wall limited (IWL), lower single null (LSN) and double null diverted (DND) boundary configurations have been produced in NSTX. Shown in Figure 1 are the equilibria obtained from the EFIT equilibrium reconstruction code. The reconstructions are based on the solutions of Grad-Shafranov equation and magnetic diagnostics (pick-up (Mirnov) coils, flux loops) measurements as described in details in [7]. Also shown in Figure 1 are the divertor D_α profiles measured by the LDIV camera. In general, the agreement between the EFIT equilibria and the camera images of plasma-surface interaction through neutral recycling or sputtered carbon brightness profiles is good. The agreement breaks down only in the marginally diverted discharges with small inner gaps and divertor magnetic null(s). Shown in Figure 2 is the comparison between EFIT strike point positions and divertor D_α emission maxima positions measured by the LDIV camera for LSN L- and H-mode plasmas. Most data points are believed to represent the "attached" divertor condition thus justifying the comparison between recycling maxima positions and the computed separatrix. The outer target strike point has a more favorable viewing geometry, and the agreement between the EFIT and optical measurements is good. The inner strike point emission frequently shows internal structure and multiple local maxima, which is believed to be the reason for the systematic discrepancy.

B. Edge particle fluxes and global confinement

Edge NSTX features resulting from the low aspect ratio geometry, namely the low toroidal field (0.3 - 0.45 T) with a large radial gradient, high mirror ratio $\max(|B|)/\min(|B|)$, large gyroradii $\rho_i \leq 2$ cm, short connection length $L \simeq \pi R q \simeq 18$ m, large SOL flux tube expansion, and compact divertor, are likely to lead to measurable edge differences with conventional tokamaks. Several tentative conclusions regarding particle flows in NSTX can

be made using particle flux order-of magnitude estimates obtained from the measured D_α brightnesses. First, the ion flux to the divertor plates in the analyzed LSN and DND discharges exceeds both the ion and neutral fluxes in the midplane by about two orders of magnitude [8], suggesting that the parallel SOL transport greatly exceeds the perpendicular (cross-field) transport. The result has a direct impact on divertor performance in ST's and will be further validated through numerical modeling. Second, large in-out asymmetries are routinely observed in heat and particle fluxes in the divertor. Higher heat and recycling fluxes are often observed on the outboard plate as in conventional tokamaks [10], due to the larger outboard surface area and the outboard particle flux enhancement linked to the compression of outboard flux surfaces. The SOL width is closely related to these asymmetries, as the inboard and outboard SOLs are connected in LSN discharges, and physically disconnected in DND discharges. This subject is of particular importance to ST's: the outboard SOL (region of bad curvature) connection length is much shorter than the inboard (good curvature) SOL connection length, and the toroidal magnetic field on the inboard side is much larger. Thus, in DND discharges inboard and outboard SOL transport may be different, whereas in LSN discharges it is expected to be similar in both regions. Characterization of SOL transport in NSTX is underway, as a fast reciprocating probe and density fluctuation diagnostics become available. Present observations of D_α inboard profiles in IWL, LSN and DND discharges are not indicative of large differences (Figure 3). Shown are the inboard D_α brightness profiles of the L-mode phase in similar 1 MA discharges with 5 MW NBI heating. The plasmas were fueled from a high field side gas injector, and a prominent feature seen on the profiles is a result of gas leakage from the inboard injector with a rate $S \leq 10$ Torr·l/s. In low field side gas fueled discharges, recycling light profiles are also often inhomogeneous with large features appearing on the center stack, however the inboard D_α profiles show weak dependence on boundary configuration.

Global particle confinement time τ_p^* can be inferred from the global particle balance equation $\frac{dN_p(t)}{dt} = -\frac{N_p(t)}{\tau_p^*} + R(t)\frac{N_p}{\tau_p^*} + \eta_g S_g + \eta_{NBI} S_{NBI}$, where $N_p(t)$ is the total particle (ion)

inventory, $R(t)N_p/\tau_p^*$ is the recycling flux from plasma-wetted surfaces, $R(t)$ being the global recycling coefficient, S_g is the gas injection rate, S_{NBI} is the NBI fueling rate, and η_g, η_{NBI} are the gas and NBI fueling efficiencies, respectively. It has been found that $\eta_g = 0.05 - 0.2$ and $\eta_{NBI} \leq 0.8$ in NSTX [8]. In the IWL configuration, neutral particle ionization occurs in the main plasma, and an estimate of the recycling flux can be obtained from D_α brightness measurements. However, the most performing NSTX plasmas with high β and high stored energy have been obtained in diverted configurations, rendering this method impractical. Detailed 2D modeling using multi-fluid and neutral transport codes will be used for the confinement analysis of divertor configurations.

C. H-mode observations

H-mode plasmas have been obtained in NSTX with either NBI or HHFW auxiliary heating in LSN and DND configurations [9]. The L-H transition is clearly visible as the D_α emission drop in the divertor and inboard midplane profiles. Shown in Figure 4 is an example of the D_α divertor profile of an LSN discharge with a short H-mode. The reversal of in-out asymmetry in recycling was observed in LSN discharges of FY 2001 campaign during ELM-free and ELMy H-mode periods. This phenomenon has not recurred in similar H-mode plasmas in the FY 2002 campaign and is believed to be related to the changes in SOL transport due to non-axisymmetric error field reduction after poloidal field coil re-alignment prior to the campaign. High temporal resolution of the cameras ($\tau \geq 208 \mu s$) enables to study the dynamics and internal structure of ELMs. "Grassy" H-mode plasmas and plasmas with type I and III ELMs have been observed. Shown in Figure 5 is a divertor D_α profile during a high field side fueled ELMy H-mode plasma heated by 1.6 MW of NBI. As evident from the figure the D_α spike associated with the mode starts by $t_{in/out} \simeq 200 \mu s$ earlier on the outboard target. The importance of ELMs in long H-mode discharges is in their potential to ameliorate impurity accumulation effects. Correlation of the time $t_{in/out}$ with H-mode edge parameters enables to study how energy and particle are transported during

ELMs to the divertor. The example given earlier is consistent with the model of conductive parallel energy transport along the outboard edge with a shorter connection length.

IV. DISCUSSION

The examples of the LDIV and MID camera measurements in NSTX given in Section III demonstrate the usefulness of simple filtered visible 1D CCD cameras for diagnosing edge plasmas. Future experiments will address the high and low field side edge transport measurements, SOL width measurements, and detailed studies of NSTX divertor regimes. Two upgrades are being planned in support of these experiments. An in-vessel mirror has been installed to enable a direct view of the outboard midplane separatrix. Also planned is a new lower divertor horizontal view enabling tomographic reconstruction of X-point region emission. Shown in Figure 6 are the planned camera views. The quality of the tomographic reconstruction is determined by the uniformity of the (p, ϕ) space sampling by detector chords, where p is the impact parameter, and ϕ is the impact angle [11]. As shown in Figure 6 the (p, ϕ) coverage of the proposed views in respect to the X-point position is fairly uniform. Because of the obstruction by the passive plates, however, the horizontal view does not include the divertor plates.

In summary, two filtered 1D CCD cameras have been fielded at NSTX. High spatial ($\delta \simeq 1$ mm) and temporal ($\tau \geq 208\mu\text{s}$) resolutions enable the detailed measurements of impurity and deuterium brightness profiles in the SOL and divertor. The obtained data provide the basis for detailed fluid modeling of core and edge particle flows and particle confinement properties of NSTX plasmas.

ACKNOWLEDGMENTS

NSTX team is acknowledged for plasma and NBI operations. Computer software support by G. Zimmer is greatly acknowledged. This research was supported by the U.S. Department

of Energy under contracts No. DE-AC02-76CH03073, DE-AC05-00OR22725, and DE-FG02-99ER54524.

REFERENCES

- [1] C. J. Boswell, J. L. Terry, B. Lipschultz, and J. Stillerman, Rev. Sci. Instrum. **72**, 935 (2001).
- [2] E. S. Marmar *et al.*, Rev. Sci. Instrum. **72**, 940 (2001).
- [3] M. E. Fenstermacher *et al.*, Rev. Sci. Instrum. **68**, 974 (1997).
- [4] J. L. Terry, J. A. Snipes, and C. Kurz, Rev. Sci. Instrum. **66**, 555 (1995).
- [5] D. A. Gates *et al.*, in *Proceedings of the 29th EPS Conference on Plasma Physics and Controlled Fusion* (Montreux, Switzerland, 2002).
- [6] M. E. Rensink *et al.*, J. Nucl. Mater. **290-293**, 706 (2001).
- [7] S. A. Sabbagh *et al.*, Nucl. Fusion **41**, 1601 (2001).
- [8] V. A. Soukhanovskii *et al.*, in *Proceedings of the 15th International Conference on Plasma Surface Interactions in Controlled Fusion Devices* (Submitted to J. Nucl. Mater., Gifu, Japan, 2002).
- [9] C. E. Bush *et al.*, Plasma Phys. Control. Fusion **44**, A323 (2002).
- [10] C. S. Pitcher and P. C. Stangeby, Plasma Phys. Control. Fusion **39**, 779 (1997).
- [11] R. S. Granetz and P. Smeulders, Nucl. Fusion **28**, 457 (1988).

[FIG. 1 about here.]

[FIG. 2 about here.]

[FIG. 3 about here.]

[FIG. 4 about here.]

[FIG. 5 about here.]

[FIG. 6 about here.]

List of Figures

1	Plasma boundary configurations (IWL, LSN, DND) reconstructed by EFIT. The lower divertor D_α profiles are shown on the same horizontal scale.	13
2	Comparison between EFIT strike point major radii R and the major radii R of D_α emission maxima measured by the LDIV camera.	14
3	Inboard midplane D_α brightness profiles measured in inner-wall limited (IWL), lower single null (LSN), upper single null (USN), and double null (DND) phase of otherwise similar discharges, fueled from a high field side gas injector.	15
4	Lower divertor D_α profile during H-mode. Recycling in-out asymmetry reversal is observed after L-H transition.	16
5	Edge localized modes in an H-mode LSN plasma.	17
6	Proposed views for X-point emission tomography and locations of CCD pixel chords in (p, ϕ) space. For clarity, only every 10th chord is shown.	18

FIGURES

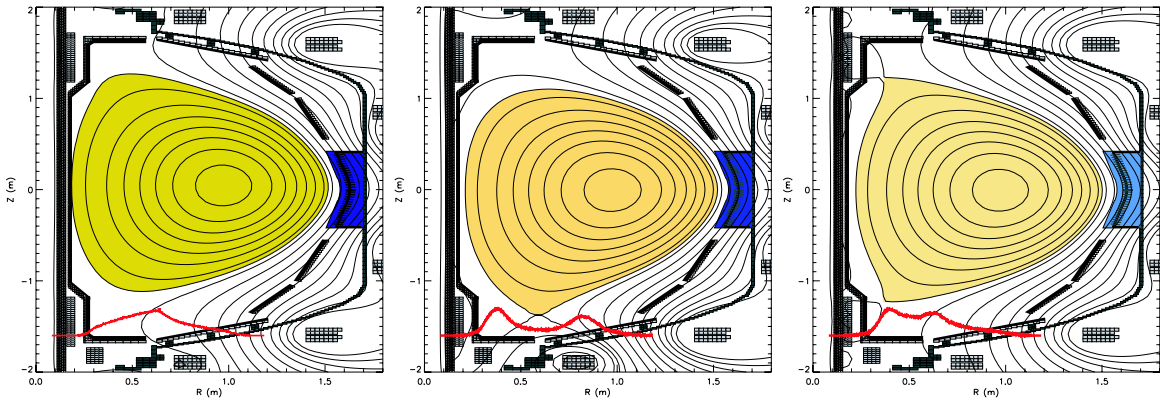


FIG. 1. Plasma boundary configurations (IWL, LSN, DND) reconstructed by EFIT. The lower divertor D_α profiles are shown on the same horizontal scale.

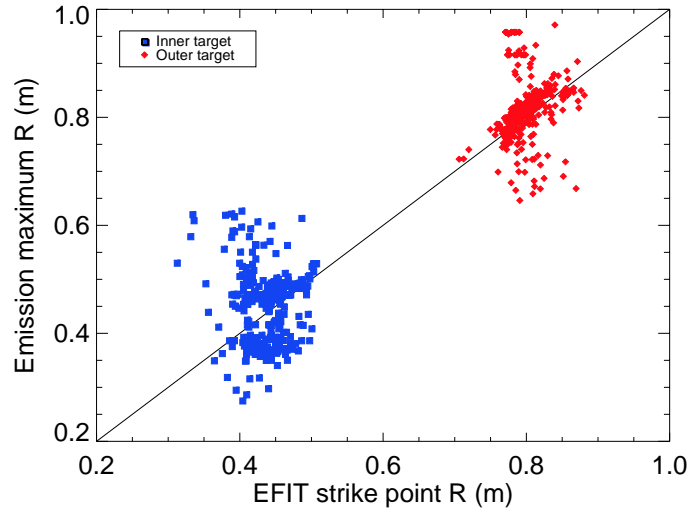


FIG. 2. Comparison between EFIT strike point major radii R and the major radii R of D_{α} emission maxima measured by the LDIV camera.

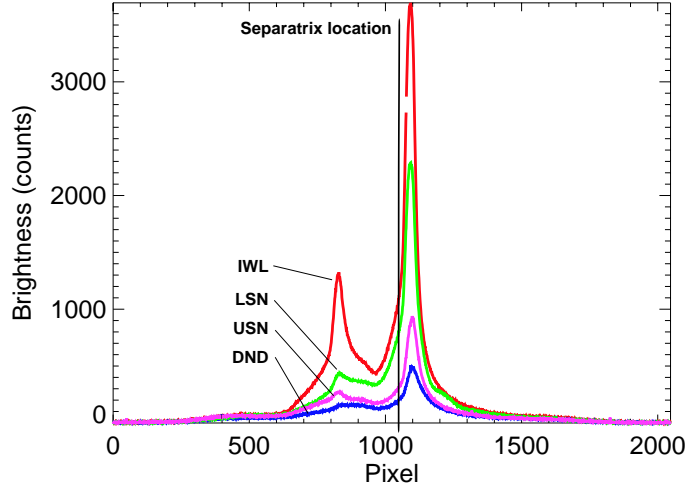


FIG. 3. Inboard midplane D_α brightness profiles measured in inner-wall limited (IWL), lower single null (LSN), upper single null (USN), and double null (DND) phase of otherwise similar discharges, fueled from a high field side gas injector.

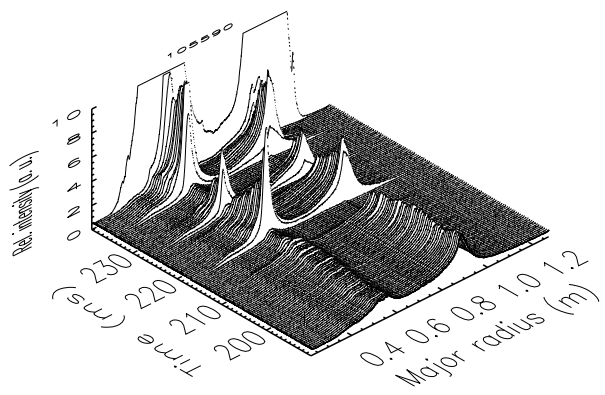


FIG. 4. Lower divertor D_α profile during H-mode. Recycling in-out asymmetry reversal is observed after L-H transition.

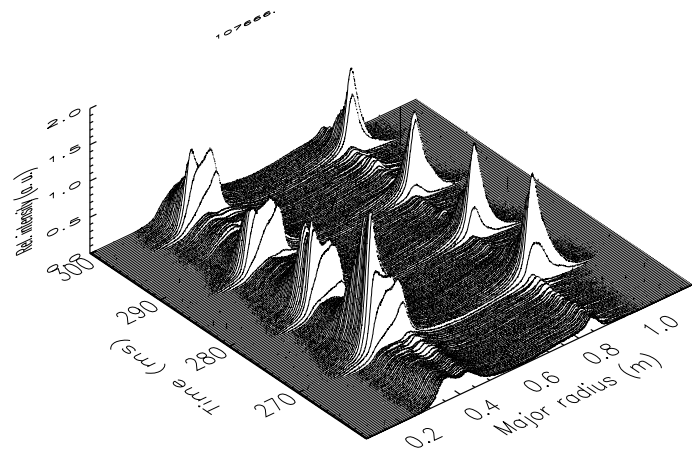


FIG. 5. Edge localized modes in an H-mode LSN plasma.

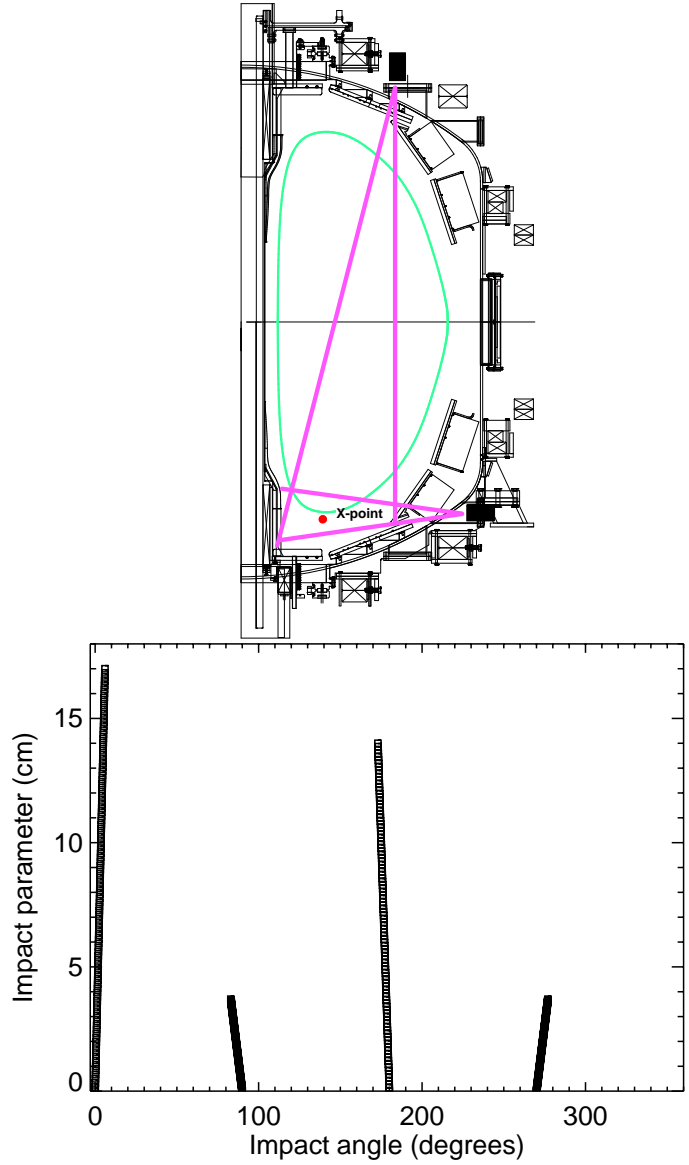


FIG. 6. Proposed views for X-point emission tomography and locations of CCD pixel chords in (p, ϕ) space. For clarity, only every 10th chord is shown.